ADVANCED MATERIALS
www.advmat.de

Polyelectrolytes as a Stable and Tunable Platform for Triboelectric Nanogenerators

Hyeonseo Joo, Sujin Park, Sujeong Gwak, Hyosik Park, Soyoung Kim, Cheoljae Lee, Wonho Lee, and Ju-Hyuck Lee**

Polyelectrolytes (PEs) provide a versatile material system for improving the efficiency and stability of triboelectric nanogenerators (TENGs). Compared to conventional ionic liquids (ILs), which suffer from leakage, environmental instability, and limited durability, PEs feature covalently tethered ionic groups that enable precise tribopolarity control while preventing unwanted ion migration. By systematically varying polymer backbones and ionic compositions, including two polycations and three polyanions, tunable triboelectric behavior is demonstrated using Kelvin Probe Force Microscopy, time-of-flight secondary ion mass spectrometry, and TENG output measurements. The polymethyl acrylate (PMA)-based polycation with 20% ion inclusion shows strongly tribopositive behavior, producing 83 V compared to 45 V for PMA. The polystyrene (PS)-based polyanion with 10% ion inclusion exhibits strongly tribonegative behavior with 34 V, compared to 8 V for PS. Optimizing ion ratios enhances charge retention by suppressing excessive ionic conduction. The mechanical and thermal stability of PEs is demonstrated by output measurements over time; for example, the short-circuit current of PMA-based polycation with 20% ion inclusion remains nearly unchanged after 1 week at 60 °C, in contrast to an ≈27% drop observed in a polymer-IL system (poly(methyl methacrylate) with 10 wt% IL). These findings highlight the suitability of PEs as a robust, stable, and tunable platform for next-generation energy-harvesting applications.

1. Introduction

Triboelectric nanogenerators (TENGs) are devices that convert irregular mechanical energy into electrical energy through triboelectrification and electrostatic induction. Their lightweight nature, ease of fabrication, reliability, and environmental friendliness make them promising renewable energy sources.[1]These characteristics render TENGs highly suitable for diverse applications, including soft robotics,[2] biomedical sensors,[3] and personal electronics.[4] Optimizing TENG performance heavily relies on selecting materials[5] with highly contrasting electron affinities to control tribopolarity, which includes both the polarity and magnitude of the charges generated during contact electrification.[6] Consequently, research in tribomaterials has been progressing rapidly, exploring various strategies to enhance the triboelectric effect, such as surface micropatterning[7] and chemical surface treatments with plasma.[8]

One of the most critical factors for enhancing TENG performance is achieving high permittivity.[9] To address this, various strategies have been introduced to increase permittivity, including the incorporation of high-dielectric fillers such as high-k nanoparticles (titanium dioxide (TiO_2),[10] barium titanate ($BaTiO_3$)[11]), conductive nanomaterial (graphene,[12] liquid metal[13]) and ionic liquids (ILs).[14] ILs, in particular, have demonstrated great potential in advancing TENGs[15] by inducing ionic polarization and significantly enhancing triboelectric charge generation through the formation of electric double layers (EDLs).[16] For instance, studies have shown that incorporating ILs into polymer matrices, such as polyurethane (PU),[14b,17] polyvinylidene fluoride (PVDF),[18] etc[16c,19] can substantially improve TENG output performance. Additionally, ILs offer advantages such as flexibility[15a,16a,20] (due to their low glass transition temperature), transparency[16a,19] (optical clarity), fire resistance[19] (from their thermally stable ionic structures), and self-healability[14a,21] (enabled by dynamic ionic interactions). These properties make IL-containing polymers highly adaptable for a wide range of applications, including wearable, transparent, and durable electronics.

However, despite their numerous advantages, traditional IL-based TENG faces critical challenges, including long-term stability, leakage risks, and environmental concerns.[22] While ILs

H. Joo, S. Gwak, H. Park, C. Lee, J.-H. Lee
Department of Energy Science and Engineering
Daegu Gyeongbuk Institute of Science and Technology (DGIST)
Daegu 42988, Republic of Korea
E-mail: jhlee85@dgist.ac.kr
S. Park, S. Kim, W. Lee
Department of Polymer Science and Engineering
Department of Energy Engineering Convergence
Kumoh National Institute of Technology
Gumi 39177, Republic of Korea
E-mail: 1holee@kumoh.ac.kr
J.-H. Lee
Energy Science and Engineering Research Center
Daegu Gyeongbuk Institute of Science and Technology (DGIST)
Daegu 42988, Republic of Korea

The ORCID identification number(s) for the author(s) of this article can be found under https://doi.org/10.1002/adma.202505547

DOI: 10.1002/adma.202505547

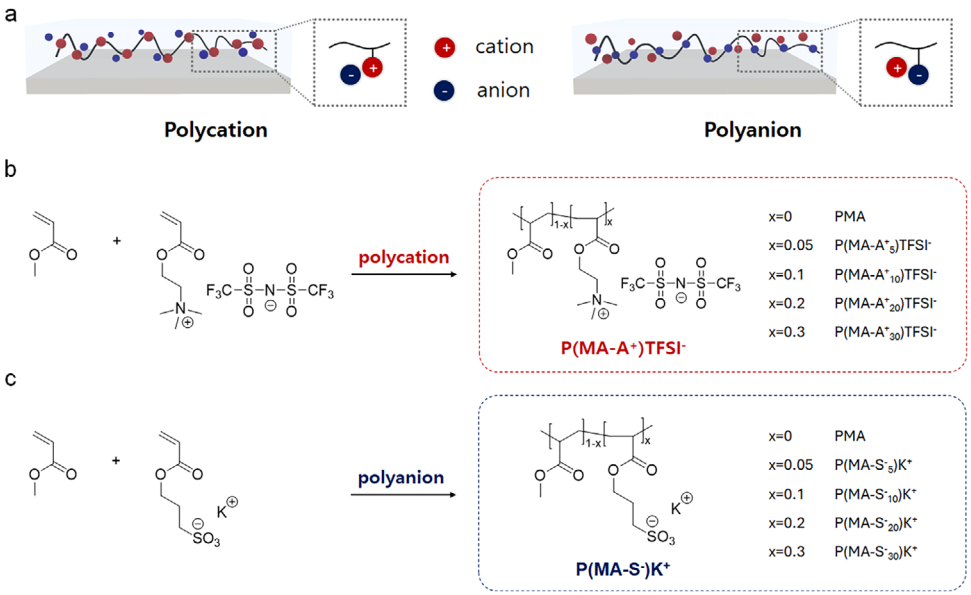

Figure 1. Overview of concept and material design of the PEs for TENGs. a) Schematic representation of the polycation and polyanion. b) The molecular structures of P(MA-A$^+$)TFSI$^-$ and c) P(MA-S$^-$)K$^+$; all PEs were synthesized with ion molar fractions of 0.05, 0.1, 0.2, and 0.3, which correspond to 5%, 10%, 20%, and 30% of the total monomer composition.

significantly enhance triboelectric charge generation through ionic polarization, their inherent sensitivity to external factors such as temperature, humidity, and oxygen can lead to evaporation or decomposition over time, ultimately degrading device performance. Additionally, ILs share similar leakage risks with electrolytes, raising concerns about potential environmental contamination. Moreover, although ILs have been widely explored in TENG applications, previous studies have not fully elucidated the influence of ionic characteristics on triboelectric behavior. The presence of both cations and anions within the polymer matrix adds further complexity to understanding charge transfer mechanisms, making it difficult to precisely control tribopolarity.[23] Therefore, a more systematic approach is required to address these limitations and unlock the full potential of IL-based materials for next-generation TENG development.

In this work, we introduce polyelectrolytes (PEs) as a novel material platform for precisely controlling tribopolarity while ensuring long-term stability in TENGs. Unlike traditional ILs, PEs incorporate covalently bonded ionic groups within a polymeric backbone, improving stability and preventing leakage while maintaining ionic polarization benefits. We systematically investigate how polymer structure and ion type (cationic or anionic) affect tribopolarity, charge generation, and mechanical/thermal stability. As a model system, we designed PEs based on polymethyl acrylate (PMA) and polystyrene (PS), varying their ionic composition to study structure-property relationships. Through a comparative analysis of two polycations and three polyanion PEs, we elucidate the relationship between ionic structure and triboelectric behavior. Furthermore, time-of-flight secondary ion mass spectrometry (TOF-SIMS) analysis is employed to explore the role of ionic polarization and charge compensation in tribopolarity modulation. This research not only deepens our understanding of IL-based TENG mechanisms but also establishes a foundation for developing stable, high-performance energy harvesting devices with tunable triboelectric properties.

2. Results and Discussion

Figure 1a presents the material design strategy for controlling triboelectric properties using PEs, where the backbone structure remains consistent while the ionic component is selectively varied. To systematically investigate the effect of ion type on triboelectric behavior, we designed PEs based on a PMA backbone, incorporating either a cationic group Poly(methyl acrylate-co-[2-(acryloyloxy)ethyl]trimethylammonium bis(trifluoromethanesulfonyl)imide) (P(MA-A$^+$)TFSI$^-$)) or an anionic group Poly(methyl acrylate-co-potassium 3-sulfopropyl acrylate) (P(MA-S$^-$)K$^+$)), as shown in Figure 1b. The synthesis of these PEs followed the routes outlined in Figure S1 (Supporting Information), with detailed procedures provided in the experimental section. By maintaining the same PMA backbone and selectively varying the ionic species, we aimed to isolate the role of ion polarity in determining tribopolarity. To further assess the effect of ionic density, varying ion incorporation ratios, specifically at molar fractions of 0.05, 0.1, 0.2, and 0.3, which correspond to 5%, 10%, 20%, and 30% of the total monomer composition. The chemical structures and the actual ratios between neutral and ionic moieties were verified via nuclear magnetic resonance (NMR) spectroscopy (Figure S2, Supporting Information), confirming successful synthesis and precise compositional control. In addition, we fabricated PE-based TENGs using the synthesized polycation and polyanion samples (Figure S3, Supporting Information) through a straightforward process involving dissolution, solution casting, drying, and device assembly. Actual images of the polyelectrolyte samples and the assembled TENG device are included for visual clarity.

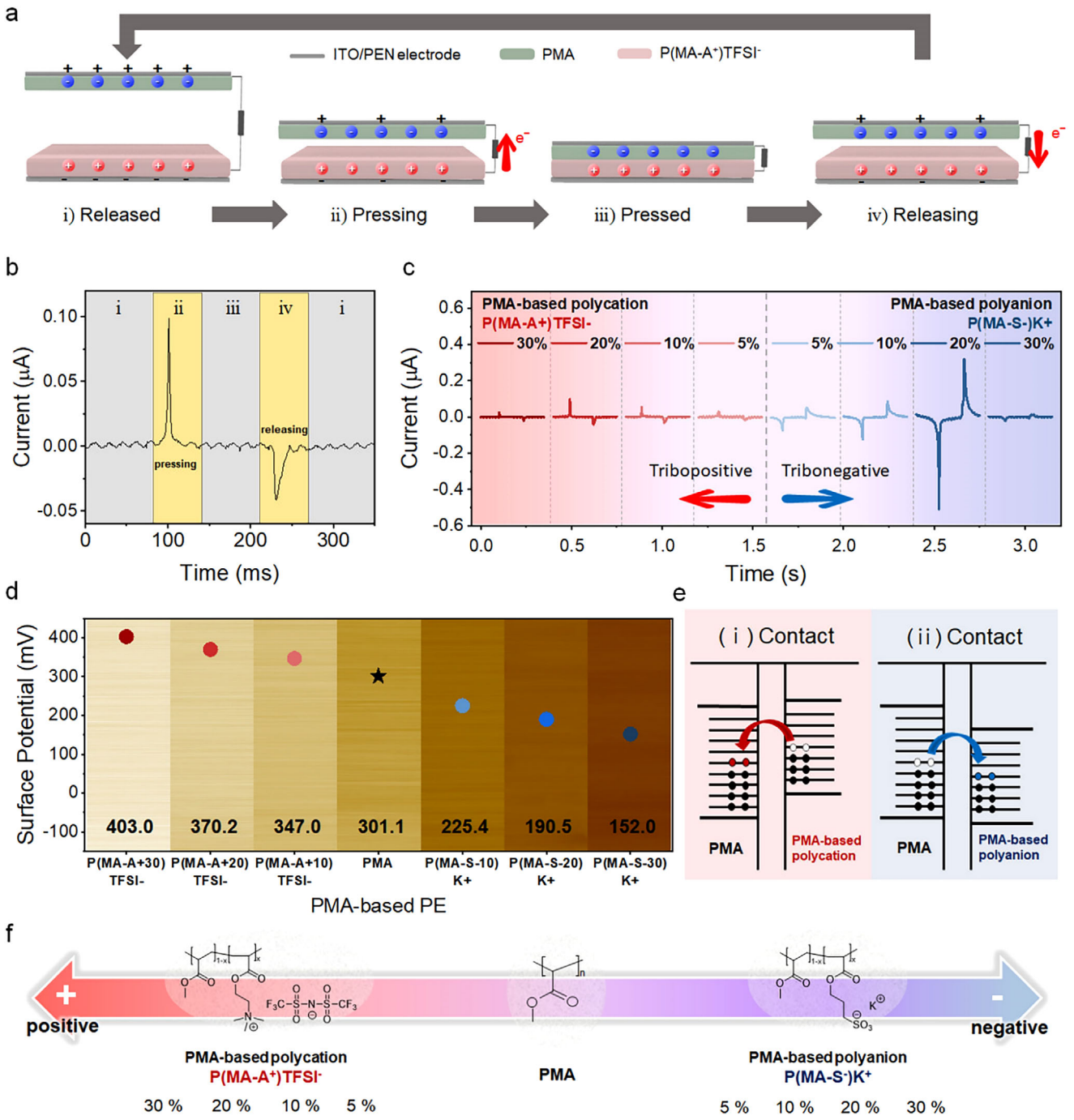

Figure 2. Tribopolarity modulation in PMA-based PEs – polycation and polyanion variants. a) Working mechanism of the P(MA-A$^+$)TFSI$^-$-based TENG in contact with PMA. b) Output voltage signal of P(MA-A$^+_{20}$)TFSI$^-$-based TENG. c) Output signal characteristics of a PMA-based PEs-triboelectric nanogenerator upon contact with PMA. d) Surface potential measurements of PMA-based PEs (P(MA-A$^+$)TFSI$^-$ and P(MA-S$^-$)K$^+$) obtained via KPFM. e) Scheme illustration of the contact charge transfer between PMA and PMA-based PEs. f) Triboelectric series for PMA-based PEs as a function of PE type and ion inclusion ratios.

Figure 2a illustrates the schematic diagram and working mechanism of TENGs utilizing PMA-based PEs (P(MA-A$^+$)TFSI$^-$) and PMA (i.e., without ionic groups) as the triboelectric layers. This setup was designed to evaluate the tribopolarity of PEs relative to the neutral PMA backbone, serving as a reference. The output current signal of P(MA-A$^+$)TFSI$^-$ based TENG is presented in Figure 2b. Initially, in the released state (step i), there is no contact between the P(MA-A$^+$)TFSI$^-$ layer and the PMA layer, resulting in no charge transfer. During pressing (step ii), the P(MA-A$^+$)TFSI$^-$ layer acquires positive charges,

while the PMA layer attains negative charges due to triboelectrification, generating a positive current signal. In the pressed state (step iii), the potential difference between the two layers is maximized, causing electron flow from the P(MA-A$^+$)TFSI$^-$ layer to the PMA layer through the external circuit. Upon releasing (step iv), as the two layers begin to separate, electrons return to the P(MA-A$^+$)TFSI$^-$ layer, producing a negative current signal. Figure 2c presents the electrical output signals observed during pressing and releasing operations. By analyzing the direction of these signals, the tribopolarity of each material can be determined.[24] A comparative analysis of PMA interactions with both P(MA-A$^+$)TFSI$^-$ and P(MA-S$^-$)K$^+$ revealed an inverse relationship in charge polarity. Specifically, P(MA-A$^+$)TFSI$^-$ exhibited enhanced tribopositive behavior, whereas P(MA-S$^-$)K$^+$ displayed stronger tribonegative behavior compared to native PMA. Notably, in both PEs with 30% ion inclusion, the output signals significantly decreased, a phenomenon that will be discussed in detail later. These results confirm that modifying the ionic composition of PEs while maintaining the same PMA backbone significantly influences tribopolarity, thereby impacting the overall output performance of TENGs.

To further clarify the triboelectric behavior of PMA-based PEs relative to neutral PMA, we compared the surface potentials of each material using Kelvin Probe Force Microscopy (KPFM). While the surface potential measured by KPFM does not precisely reflect the effective work function due to various external influences, it serves as a reliable comparative tool for assessing triboelectric trends among materials by evaluating relative differences. As shown in Figure 2d, surface potential measurements revealed a clear correlation between ion concentration and triboelectric properties. Neutral PMA exhibited a surface potential of ≈301 mV, serving as the reference. In contrast, P(MA-A$^+$)TFSI$^-$ showed a gradual increase, reaching 403 mV at its highest ion ratio (P(MA-A$^+_{30}$)TFSI$^-$), indicating enhanced tribopositivity. Conversely, P(MA-S$^-$)K$^+$ displayed a systematic decrease, dropping to 152 mV at P(MA-S$^-_{30}$)K$^+$, highlighting the role of ion composition in modulating triboelectric behavior. These results suggest a charge transfer mechanism dictated by the electronic states of the materials. When PMA-based polycation (P(MA-A$^+$)TFSI$^-$) contacts neutral PMA, electron transfer occurs from the filled electronic states of P(MA-A$^+$)TFSI$^-$ to the empty electronic states of PMA (Figure 2e(i)). In contrast, when PMA-based polyanion (P(MA-S$^-$)K$^+$) interacts with PMA, electron flows from PMA to P(MA-S$^-$)K$^+$ (Figure 2e(ii)), leading to tribonegative behavior. Figure 2f summarizes these findings, demonstrating that P(MA-A$^+$)TFSI$^-$ exhibits progressively stronger tribopositive behavior with increasing ion concentration, whereas P(MA-S$^-$)K$^+$ becomes increasingly tribonegative under similar conditions. These results highlight the tunability of triboelectric properties through controlled ionic modifications in PEs, offering a systematic approach for optimizing TENG performance. To further confirm the tunable triboelectric behavior of PMA-based PEs, we conducted a comparative analysis between the materials, as shown in Figure S4 (Supporting Information). With increasing ion content, P(MA-A$^+$)TFSI$^-$ samples exhibited progressively stronger tribopositive behavior, while P(MA-S$^-$)K$^+$ samples became more tribonegative. These results align with the triboelectric series shown in Figure 2f, confirming the influence of ionic composition on tribopolarity.

To systematically evaluate the triboelectric performance of P(MA-A$^+$)TFSI$^-$ and P(MA-S$^-$)K$^+$, we fabricated TENGs using nylon, polyethylene terephthalate (PET), polyimide (PI), and perfluoroalkoxy alkane (PFA) as counter materials and measured their output performance. Given the well-established triboelectric ranking of these materials (Figure S5, Supporting Information), this experimental design allowed for a relative assessment of PE-based tribopolarity across different counter materials. As shown in **Figure 3a**, when using nylon, which is a conventional tribopositive material, neutral PMA exhibited slightly tribopositive behavior, generating an output voltage of ≈5 V. However, P(MA-A$^+_{20}$)TFSI$^-$ demonstrated significantly enhanced tribopositivity, reaching 59 V, whereas P(MA-S$^-$)K$^+$ became increasingly tribonegative, reversing its output signal beyond a 10% ion ratio and peaking at ≈−36 V at 20% ion inclusion. A similar trend was observed with other counter materials, including PET, PI, and PFA, as shown in Figure 3b,c, and Figures S6–S9 (Supporting Information), including detailed output data (voltage, current, and normalized charge density, μC m^{-2}). Across all cases, the relative positioning of PEs within the triboelectric series (Figure 3d) determined the polarity and magnitude of charge transfer, confirming that ionic composition and counter-material selection systematically control tribopolarity. Notably, P(MA-A$^+_{20}$)TFSI$^-$ consistently exhibited stronger tribopositive behavior relative to nylon, PET, PI, and PFA, while P(MA-S$^-_{20}$)K$^+$ became increasingly tribonegative compared to PET and nylon but remained tribopositive relative to PI and PFA. This behavior can be attributed to the limited tribonegative potential of the PMA backbone, which restricts the extent of negative charge transfer. Furthermore, the peak output for all counter materials occurred at a 20% ion ratio, suggesting an optimal balance between charge generation and stability. This is because higher ion concentrations lead to increased ionic conductivity, causing leakage current and reduced output (as further discussed in Figure 3h). These findings establish PMA-based PEs as tunable triboelectric materials, capable of being positioned anywhere within the triboelectric series by adjusting their ionic ratios and counter-material pairings. This tunability enables precise control over tribopolarity, offering a versatile strategy for optimizing TENG performance in diverse material systems. We further evaluated the long-term performance stability by tracking current density over time using nylon as the counter material and P(MA-A$^+_{20}$)TFSI$^-$ and P(MA-S$^-_{20}$)K$^+$ as the active layers (Figure 3e). The stability results indicate that both the tribopositive and tribonegative states maintain consistent and stable outputs over an extended period, demonstrating the reliability of PMA-based PEs.

To further investigate the impact of ion inclusion on triboelectric performance, we analyzed the dielectric constant and conductivity of P(MA-A$^+$)TFSI$^-$ and P(MA-S$^-$)K$^+$ as functions of the ion inclusion ratio. Figure 3f,g show that the dielectric constant, measured at 3 Hz, increases significantly with higher ion inclusion ratios for both polycation and polyanion systems, which can be attributed to the ionic polarization effect. This enhancement in the dielectric constant likely supports increased surface charge density,[25] correlating with the higher output voltage observed at 20% ion inclusion (Figure 3a). While a higher dielectric constant contributes to improved charge density, the overall triboelectric performance is predominantly governed by tribopolarity shifts. For example, with PET and PFA (Figure 3b,c), the output

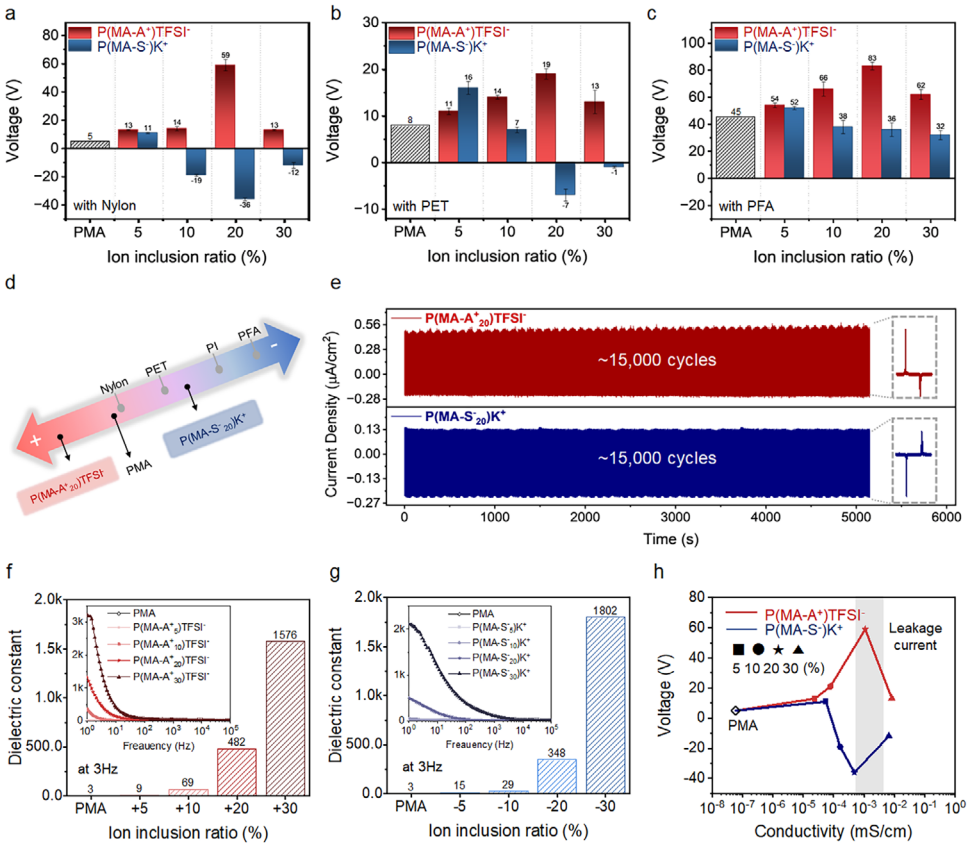

Figure 3. Output performance and electric properties of PMA-based polycation and polyanion. (Contact area: 3 × 3 cm^2, Frequency: 3 Hz, Force: 20 N, 25 °C, 40% RH) Open-circuit voltage of PMA-based PEs ($P(MA\text{-}A^+)TFSI^-$ and $P(MA\text{-}S^-)K^+$) TENG as a function of ion inclusion ratio in contact with a) nylon, b) PET and, c) PFA. d) Comparison of triboelectricity between $P(MA\text{-}A^+_{20})TFSI^-$/$P(MA\text{-}S^-_{20})K^+$ and other polymers (nylon, PET, PI, and PFA). e) Long term stability $P(MA\text{-}A^+)TFSI^-$ and $P(MA\text{-}S^-)K^+$ based TENGs contact with nylon. The dielectric constant of PMA-based PEs was measured at 3 Hz, for f) $P(MA\text{-}A^+)TFSI^-$ and g) $P(MA\text{-}S^-)K^+$. h) Relationship between output voltage and ionic conductivity of $P(MA\text{-}A^+)TFSI^-$ and $P(MA\text{-}S^-)K^+$, measured using nylon as the counter material.

of $P(MA\text{-}S^-)K^+$ shows a clear decreasing trend as the ion inclusion ratio increases. This behavior is primarily attributed to the increasingly tribonegative nature of the polyanion system, which suppresses charge transfer at higher ion ratios. In contrast, polycation systems maintain tribopositive behavior, peaking at 20% before declining. These results confirm that tribopolarity shifts induced by varying ion inclusion ratios are the primary determinant of output performance.

Additionally, at 30% ion inclusion, a significant decrease in output voltage is observed across all systems (Figure 3a–c). To evaluate whether this reduction originates from mechanical properties, especially brittleness induced by excessive ion inclusion, we performed rheological measurements to obtain shear storage and loss modulus data. Figure S10 (Supporting Information) presents oscillatory shear sweeps conducted from 1 to 100 rad s^{-1}, with the storage modulus, loss modulus, and tan δ (loss factor) summarized at 1 rad s^{-1}. Interestingly, polycation and polyanion systems exhibit opposite trends. The storage modulus of the polycation decreases with increasing ion composition, while that of the polyanion increases. Furthermore, their tan δ also shows distinct behavior; specifically, the tan δ of the polycation increases with higher ion ratios. These contrasting trends arise from differences in ionic structures and intermolecular interactions. In the polycation system, bulky counter-anions ($TFSI^-$) inhibit the formation of ionic clusters, reducing intermolecular interactions. Conversely, small-sized K^+ ions in the polyanion system facilitate stronger intermolecular interactions by promoting ionic cluster formation.[26] Based on these observations, we can conclude that variations in mechanical properties do not significantly impact TENG performance. Instead, the performance decline at 30% ion inclusion is mainly attributed to leakage current, which becomes prominent when conductivity exceeds ≈10^{-3} mS cm^{-1}.[19] Conductivity analysis confirms that both $P(MA\text{-}A^+_{30})TFSI^-$ and $P(MA\text{-}S^-_{30})K^+$ surpass this threshold, leading to suppressed output (Figure 3h). As shown in Figure S11 (Supporting Information), higher ion concentrations at 30% inclusion lead to the formation of leakage pathways, which significantly suppress output performance. This highlights the need to carefully balance ion ratios to optimize TENG performance.

The phenomenon of polycations becoming tribopositive and polyanions becoming tribonegative can be attributed to the behavior of ions in PEs. In these systems, either the cation or anion is anchored to the polymeric backbone, while the counterions remain free to migrate. This configuration causes the counterions to localize at the surface, establishing a stable ionic polarization as the mobile ions move and accumulate. This

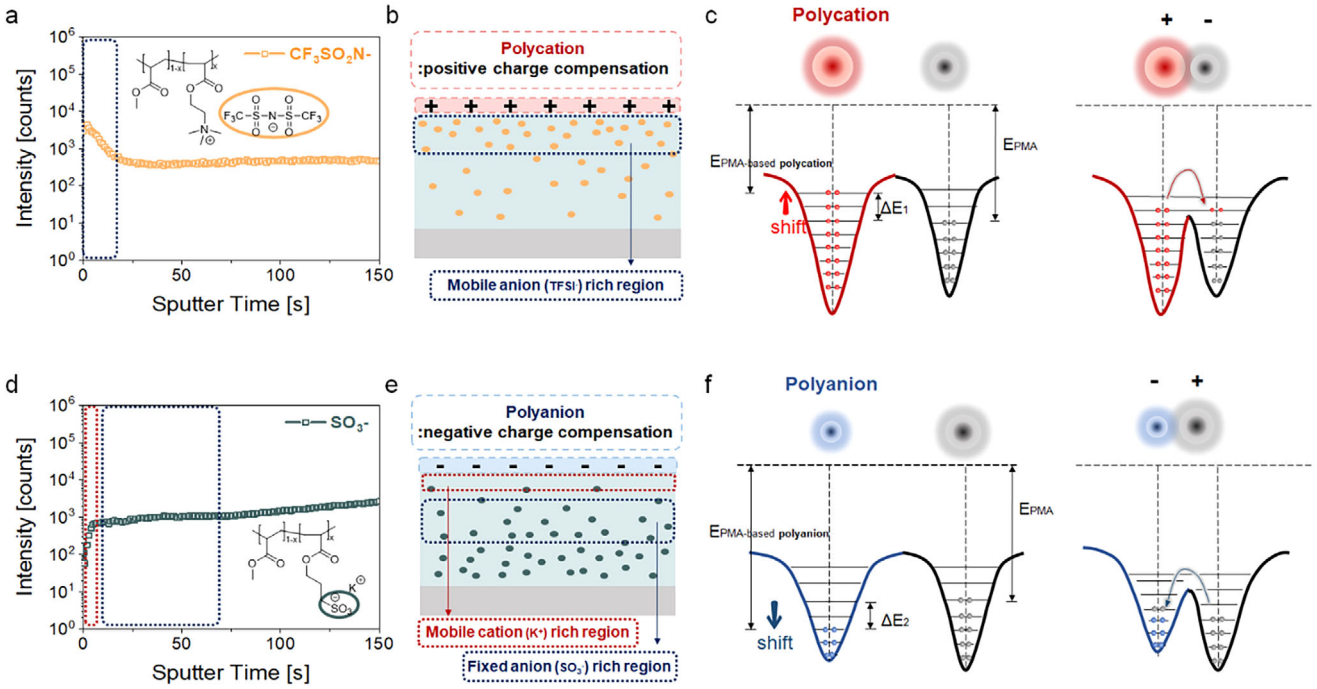

Figure 4. The working mechanism of polyelectrolyte-based TENG. a) TOF-SIMS depth profiles of negative ion ($CF_3SO_2N^-$) from P(MA-A^+)$TFSI^-$. b) Migration and accumulation of free ions and the formation of internal ionic polarization in polycation. c) The overlapped electron-cloud model for polycation and transfer of charge. d) TOF-SIMS depth profiles of negative ion (SO_3^-) from P(MA-S^-)K^+. e) Migration and accumulation of free ions and the formation of internal ionic polarization in polyanion. f) The overlapped electron-cloud model for polyanion and transfer of charge.

process enhances triboelectric charge accumulation through the formation of compensating charges, thereby improving TENG output performance. To investigate and elucidate this phenomenon, time-of-flight secondary ion mass spectrometry (TOF-SIMS) was employed to analyze the presence and distribution of ions near the surface. **Figure** 4a presents the TOF-SIMS depth profiles for CF_3SO_2N- in P(MA-A^+_{20})$TFSI^-$ after sputtering the surface for ≈150 s, revealing that mobile anions are more concentrated at the surface than in the bulk. This preferential migration of mobile anions toward the surface leads to localized charge redistribution. As shown in Figure 4b and Figure S12a (Supporting Information), the migration of $TFSI^-$ anions to the surface is evident from the increased $CF_3SO_2N^-$ signal in the TOF-SIMS depth profile, while the fixed cations remain in the bulk. This redistribution induces internal ionic polarization and charge compensation, stabilizing a net positive charge at the interface, which in turn results in the polycation exhibiting tribopositive characteristics. To further illustrate this behavior, Figure 4c depicts the electronic interaction between the PMA-based polycation and PMA upon contact. The surface accumulation of mobile $TFSI^-$ anions, as observed through TOF-SIMS, likely affects the polycation's energy levels, potentially facilitating electron transfer to PMA. Upon separation, the transferred electrons become confined by potential barriers, leading to a stable positive charge on the polycation surface, thereby reinforcing its tribopositive behavior.

Conversely, P(MA-S^-)K^+ showed the opposite behavior: mobile cations (K^+) preferentially migrate toward the surface, as confirmed by TOF-SIMS depth profiles of SO^{3-} in P(MA-S^-)K^+ shown in Figure 4d. As shown in Figure 4e and Figure S12b (Supporting Information), this redistribution induces internal ionic polarization, with charge compensation occurring due to the accumulation of mobile cations at the surface. This charge imbalance enhances the polyanion's tendency to attract electrons upon contact, stabilizing a net negative charge and reinforcing its tribonegative behavior. Figure 4f further illustrates the electronic interaction between the PMA-based polyanion and PMA upon contact. The surface-localized mobile cations likely induce a downward shift in energy levels, making the polyanion energetically favorable for electron acceptance from PMA. Upon separation, potential barriers restrict the return of the transferred electrons, resulting in a stable negative charge on the polyanion surface and further strengthening its tribonegative behavior.

To verify the universality of PE structural effects on the tribopolarity across different material configurations, we explored variations in ion types and polymeric backbones to assess their influence on triboelectric behavior (**Figure** 5a). Specifically, we analyzed the impact of replacing the polyanion in P(MA-A^+)$TFSI^-$ with imidazole (poly(methyl acrylate-co-1-(2-acryloyloxyethyl)-3-methylimidazolium bis(trifluoromethanesulfonyl)imide) (P(MA-I^+)$TFSI^-$)) and substituting the counterion in P(MA-S^-)K^+ with imidazole (poly(methyl acrylate-co-1-ethyl-3-methylimidazolium 3-sulfopropyl acrylate) (P(MA-S^-)I^+)) on triboelectric behavior. Additionally, we investigated the effect of replacing the PMA polymeric backbone with PS (poly(styrene-co-sodium 4-vinylbenzenesulfonate) (P(S-S^-)Na^+)) to further evaluate the structural dependence of triboelectric properties. The synthetic schemes of PMA-based imidazole PEs and PS-based PEs are outlined in Figure S13 (Supporting Information), with detailed procedures provided in the experimental section.

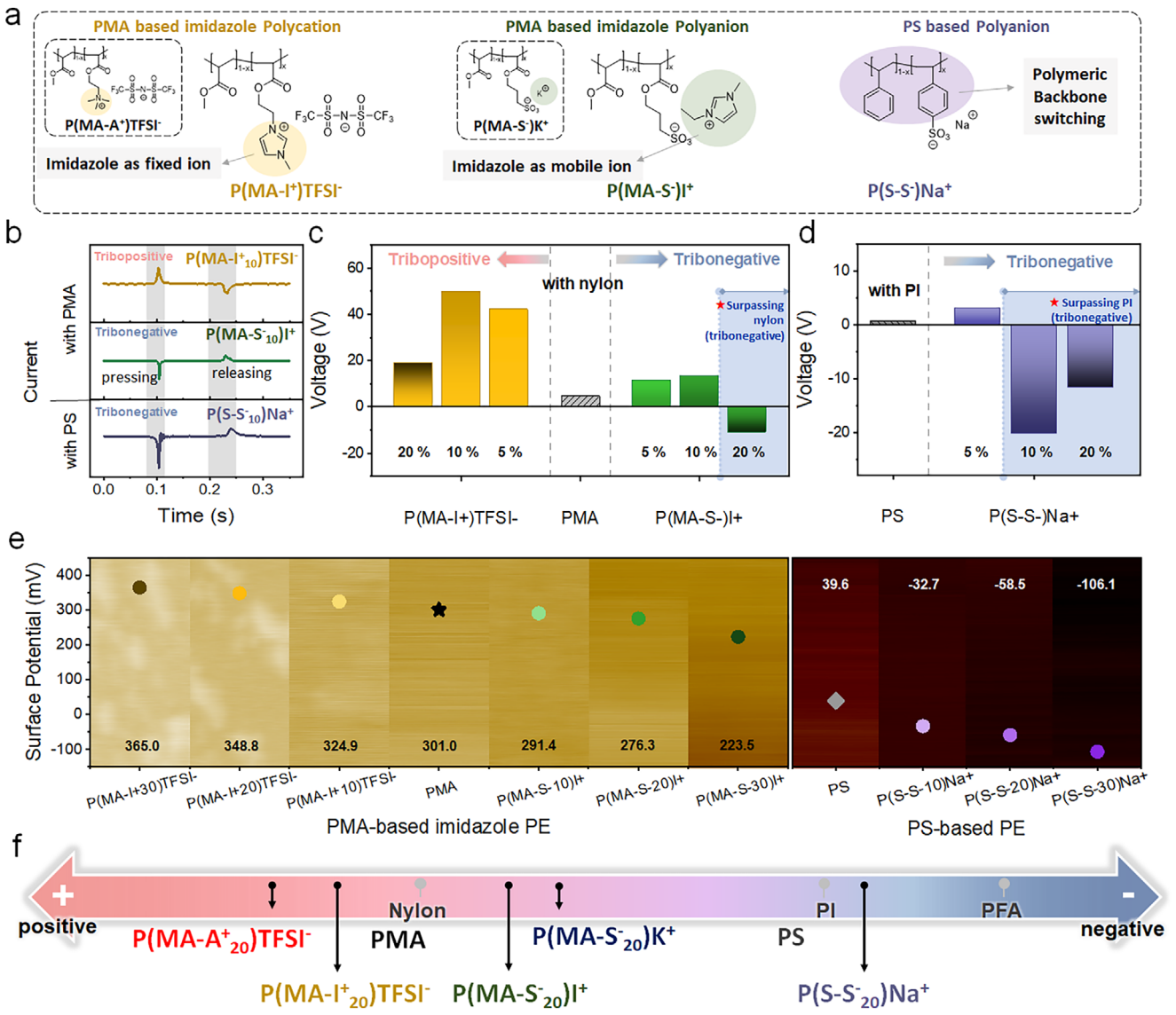

Figure 5. Modulation of tribopolarity by change of type of ions and backbone modification in PEs. a) The molecular structures of PMA-based imidazole PEs and PS-based PE. b) Output signal characteristics of TENGs upon contact with PMA and PS. c) Output signal characteristics of a PMA-based imidazole PE-TENG upon contact with nylon. d) Output signal characteristics of a PS-based PE-TENG upon contact with PI. e) Surface potential measurements of PEs ($P(MA\text{-}I^{+})TFSI^{-}$, $P(MA\text{-}S^{-})I^{+}$ and $P(S\text{-}S^{-})Na^{+}$) obtained through KPFM. f) Triboelectric series for PEs ($P(MA\text{-}A^{+}_{20})TFSI^{-}$, $P(MA\text{-}I^{+}_{20})TFSI^{-}$, $P(MA\text{-}S^{-}_{20})K^{+}$, $P(MA\text{-}S^{-}_{20})I^{+}$, and $P(S\text{-}S^{-}_{20})Na^{+}$).

The chemical structures and their ion ratios of the PMA-based imidazole PEs were confirmed using NMR spectroscopy (Figure S14, Supporting Information). For the PS-based polyanion, the ion ratios were determined through elemental analysis (EA), as the chemical shifts in the neutral and ionic segments were identical (Table S1, Supporting Information).

Figure 5b demonstrates the output electrical signals during pressing and releasing operations for $P(MA\text{-}I^{+})TFSI^{-}$ and $P(MA\text{-}S^{-})I^{+}$ in contact with PMA. Consistent with previous observations, $P(MA\text{-}I^{+})TFSI^{-}$ exhibits tribopositive behavior, generating a positive current, while $P(MA\text{-}S^{-})I^{+}$ exhibits tribonegative behavior, producing a negative current (Figure S15, Supporting Information). Similarly, when $P(S\text{-}S^{-})Na^{+}$ was tested in contact with PS, it exhibited a tribonegative behavior, consistent with that of other polyanions, including $P(MA\text{-}S^{-})K^{+}$ and $P(MA\text{-}S^{-})I^{+}$ (Figure S16, Supporting Information). Figure 5c,d show the output performance of PMA-based imidazole PE and PS-based PE when in contact with conventional triboelectric layers such as nylon and PI, respectively. The triboelectric output performance also strongly depends on ion concentration, similar to the results shown in Figures 2 and 3. $P(MA\text{-}S^{-})I^{+}$ (polyanion) becomes increasingly tribonegative as ion content increases, surpassing nylon in tribonegativity at 20%. Meanwhile, $P(MA\text{-}I^{+})TFSI^{-}$ (polycation) exhibits enhanced TENG output and becomes more tribopositive with increasing ion concentration. However, beyond 20%, the output decreases due to increased conductivity, following a trend similar to other PEs in Figure 3 (Figures S17–S20, Supporting Information). Additionally, while native PS exhibits

a more tribopositive characteristic compared to PI, the polyanion structure (P(S-S$^-$)Na$^+$) becomes more tribonegative than PI when the ion concentration exceeds 10% (Figures S21–S24, Supporting Information). These findings confirm that ionic composition and triboelectric polarity are closely linked, with polycations exhibiting tribopositive behavior and polyanions displaying tribonegative behavior. This trend persists across different ion types and polymeric backbones, demonstrating the broad applicability of our approach. Furthermore, surface potential analysis (Figure 5e) reveals that P(MA-I$^+$)TFSI$^-$ shows increased tribopositivity with higher ion ratios, reaching 365 mV at 30%. Conversely, P(S-S$^-$)Na$^+$ becomes more tribonegative, decreasing to −106 mV, emphasizing the critical role of ion concentration in modulating triboelectric properties. As shown in Figure 5f and Figure S25 (Supporting Information), the triboelectric series can be established for these materials using the 20% ion inclusion samples (P(MA-A$^+_{20}$)TFSI$^-$, P(MA-I$^+_{20}$)TFSI$^-$, P(MA-S$^-_{20}$)K$^+$, P(MA-S$^-_{20}$)I$^+$, and P(S-S$^-_{20}$)Na$^+$), with polycations positioned toward the tribopositive behavior and polyanions toward the tribonegative behavior. These results underscore that both ion selection and polymeric backbone significantly influence triboelectric behavior. This tunability offers significant advantages for the design and development of high-performance TENGs. Although the output performance of our TENGs is relatively modest, the ability to systematically control tribopolarity through ionic composition and polymeric structure offers a unique and practical advantage. Table S2 (Supporting Information) presents a comparison with previously reported ionic polymer-based systems, underscoring the tunable platform established in this work.

Next, we explored the mechanical and thermal stability of PE systems by measuring the output of P(MA-A$^+_{2n}$)TFSI$^-$ under applied forces ranging from 10 N to 40 N and at different temperatures. As shown in **Figure 6**a,b, and P(MA-A$^+_{2n}$)TFSI$^-$ maintained stable performance without any reduction in output, even after one week of storage at 60 °C and under various pressure conditions. Notably, the measurements in Figure 6b were conducted using a hotplate for temperature control, demonstrating the measurement process under high-temperature conditions (Video S1, Supporting Information). Additionally, the long-term stability analysis revealed that the samples retained their stable output both in the original state and after storage, further confirming that the PE structure ensures mechanical and thermal stability. Subsequently, we compared the stability of traditional polymer-IL systems, which consist of a polymer matrix and freely mobile ILs, with PEs. To make this comparison, we prepared a polymer electrolyte using poly(methyl methacrylate) (PMMA) and 1-Ethyl-3-methylimidazolium bis(trifluoromethylsulfonyl)imide ([EMIM][TFSI]) (Figure S26a, Supporting Information). As shown in Figure S26b (Supporting Information), the voltage and current outputs for PMMA with ILs demonstrate initial improvements. However, as the ion ratio increases to 20 wt%, the material becomes sticky and unsuitable for effective TENG operation, making it impossible to measure output performance. Therefore, we utilized 10 wt% IL-infused PMMA as a control sample, which contained a smaller amount of IL compared to the PEs.

To further compare the stability of PEs and polymer-IL systems, we tested PMMA with 10 wt% IL (PMMA+10IL) under applied forces ranging from 10 to 40 N (Figure 6d). After one week of storage at 60 °C, the overall output of PMMA+10IL decreased significantly compared to its original state, with a greater reduction observed at higher applied forces. Furthermore, when measured at 60 °C (Figure 6e; Video S2, Supporting Information), the output increased for applied forces of 10 N to 30 N compared to measurements taken at room temperature (RT). This increase is attributed to the enhanced mobility of ILs at elevated temperatures.[21] However, at an applied force of 40 N, the output decreased below that at RT. After one week of storage at 60 °C, the output exhibited an even more pronounced decrease. These results suggest that the polymer-IL TENG is highly susceptible to performance issues under high temperature and mechanical stress due to leakage.[27] In contrast, the PE-based TENG maintained stable operation even under similar conditions. Moreover, long-term stability analysis (Figure 6c,f) revealed that the PE-based TENG operated consistently at RT both before and after one week of storage at 60 °C. In comparison, the polymer-IL TENG showed a reduced output after storage at 60 °C and failed to recover its performance over extended measurements, again due to IL leakage during storage. These findings highlight PEs as a robust and tunable platform for developing high-performance TENGs. To further confirm the environmental robustness of PEs, we investigated their stability under varying humidity conditions (40%, 60%, and 80% RH). As shown in Figure S27 (Supporting Information), the output current of P(MA-A$^+_{20}$)TFSI$^-$ remained consistent across all tested humidity levels, demonstrating the negligible impact of humidity on its triboelectric performance. This result further supports the reliability of PEs under diverse environmental conditions.

In addition, we investigated the interaction mechanisms within the PE and polymer-IL systems, as illustrated in Figure 6g,h. Specifically, in PEs (Figure 6g), the ionic components are strongly bound to the polymer backbone via ion–dipole interactions, which ensure structural stability and minimize ion leakage. In contrast, the polymer-IL system (Figure 6h) exhibits weaker ion interactions, with ionic species remaining more mobile within the polymer matrix. This difference accounts for the superior thermal and mechanical stability of PEs, as confirmed by the long-term performance data in Figure 6c,f.

To further demonstrate the versatility of our PE-based TENGs, we explored their performance across various operational modes. Specifically, we fabricated TENGs using P(MA-A$^+_{20}$)TFSI$^-$ as the polycation and P(S-S$^-_{10}$)Na$^+$ as the polyanion and evaluated their performance in single-electrode mode (Figure S28, Supporting Information), lateral-sliding mode (Figure S29, Supporting Information), and freestanding triboelectric-layer mode (Figure S30, Supporting Information). These experiments confirmed that the PE-based TENGs can operate consistently across different TENG configurations, highlighting their broad applicability. This versatility suggests that our PE-based TENG platform can be widely adopted in diverse energy-harvesting applications.

3. Conclusion

We propose a new strategy for controlling tribopolarity by tailoring polymeric backbones and adjusting the fixed or mobile ions in PEs. Through KPFM and TENG analysis, we demonstrate that polycations exhibit increasingly tribopositive behavior, while polyanions become more tribonegative as ion ratios

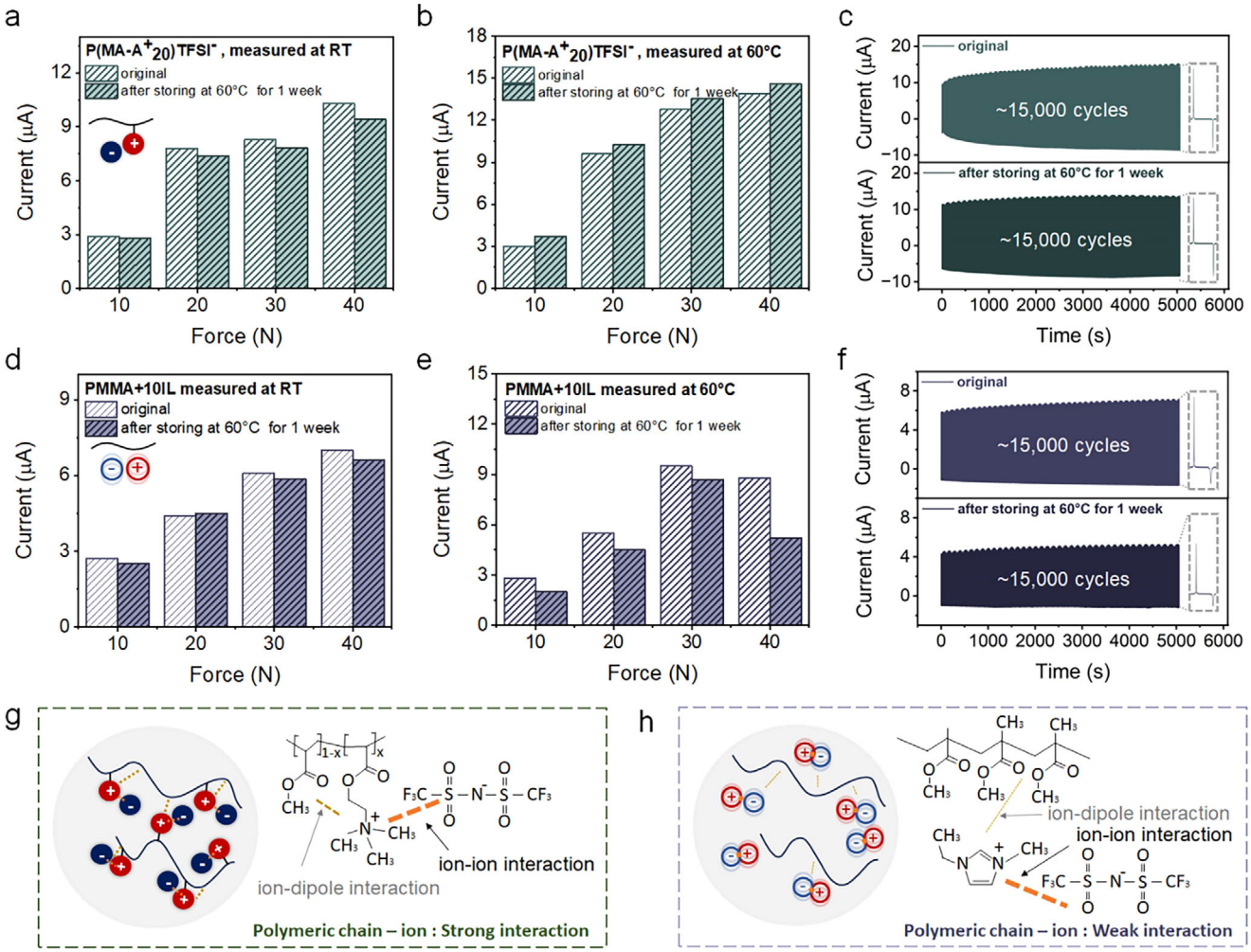

Figure 6. a) Short-circuit current of P(MA-A^+_{20})$TFSI^-$ measured at RT (40% RH) in the original state and after storing at 60 °C. b) Short-circuit current of P(MA-A^+_{20})$TFSI^-$ measured at 60 °C in the original state and after storing at 60 °C. c) Long-term stability of P(MA-A^+_{20})$TFSI^-$ (with PFA) at RT (40% RH) in the original state and after storing at 60 °C. (with PFA, Contact area: 3 × 3 cm^2, Frequency: 3 Hz, Force: 20 N) d) Short-circuit current of PMMA+10IL measured at RT (40% RH) in the original state and after storing at 60 °C. e) Short-circuit current of PMMA+10IL measured at 60 °C in its original state and after storing at 60 °C. f) Long-term stability of PMMA+10IL (with PFA) at RT (40% RH) in the original state and after storing at 60 °C (with PFA, Contact area: 3 × 3 cm^2, Frequency: 3 Hz, Force: 20 N). Schematic representation of possible non-covalent interactions (g) in PEs system and (h) in Polymer-ionic liquids systems.

increase. This systematic modulation of tribopolarity enhances our understanding of the triboelectric series and contributes to improved TENG performance. Furthermore, TOF-SIMS analysis provides deeper insights into the fundamental mechanisms governing tribopolarity in PEs, particularly the role of mobile ions in surface charge redistribution. These findings establish a solid foundation for the rational design of next-generation tribomaterials. Beyond their triboelectric properties, PEs exhibit excellent mechanical and thermal stability under various stress conditions, maintaining consistent performance even after prolonged exposure to elevated temperatures and mechanical forces. With their tunable tribopolarity, PEs offer a versatile and durable platform for high-performance TENGs. This work paves the way for advanced energy harvesting and sensing technologies, broadening the applicability of PE-based materials in sustainable energy solutions.

4. Experimental Section

Materials: N,N-Dimethylformamide (DMF, 99.9%), dimethyl sulfoxide (DMSO, 99.5%), toluene (99.5%), methyl acrylate (MA), styrene (S), and 2,2-azobisisobutyronitrile (AIBN) were purchased from Daejung Chemicals. Poly(methyl methacrylate) (PMMA), 1-Ethyl-3-methylimidazolium bis(trifluoromethylsulfonyl)imide ([EMIM][TFSI]) and [2-(Acryloyloxy)ethyl]trimethylammonium chloride solution was purchased from Sigma–Aldrich. 3-(acryloyloxy)propane-1-sulfonate (2) was purchased from BLD Pharmatech Ltd. Lithium bis(trifluoromethanesulfonyl)imide (LiTFSI), 1-methylimidazole, sodium 4-vinylbenzene sulfonate (5), and 1-ethyl-3-methylimidazolium chloride were purchased from TCI. Potassium 2-bromoethyl acrylate was purchased from Angene. MA and S were used after purification to remove inhibitors.

Synthesis of Monomers: P(MA-A^+)$TFSI^-$ monomer ([2-(acryloyloxy)ethyl]trimethylammonium bis(trifluoromethanesulfonyl)imide) (1): A solution of [2-(acryloyloxy)ethyl]trimethylammonium chloride solution

(1 eq) and LiTFSI (1.5 eq) was prepared in DI water. The reaction mixture was stirred overnight at RT. The crude product was extracted and washed with DCM and DI water, respectively. The solution was dried over anhydrous $MgSO_4$ and the solvent was removed via a rotary evaporator. After drying, a viscous transparent oil product was obtained. ^{1}H NMR (400 MHz, DMSO-d_6): 6.37-5.91 (m, 3H, CH_2═CH—), 4.51 (t, 2H, —O—CH_2—), 3.69 (t, 2H, —O—CH_2—CH_2—N), 3.17 (s, 9H, —N—$(CH_3)_3$).

P(MA-I^+)$TFSI^-$ monomer (1-(2-acryloyloxyethyl)-3-methylimidazolium bis(trifluoromethanesulfonyl)imide) (3): compound 3 was synthesized by modifying a previous research paper.[28] Under the N_2 atmosphere, 2-bromoethyl acrylate (1 eq) and 1-methylimidazole (1.2 eq) were dissolved in MeCN and refluxed overnight. After the reaction, MeCN was removed via a rotary evaporator. The intermediate was extracted from DI water and washed by DCM. Then, LiTFSI (1 eq) was added to the extracted aqueous solution and stirred overnight at RT. The crude product was extracted and washed with DCM and DI water, respectively. The solution was dried over anhydrous $MgSO_4$ and the solvent was removed via a rotary evaporator. After drying, a yellowish transparent oil product was obtained. ^{1}H NMR (400 MHz, DMSO-d_6): 9.13 (s, 1H, H2 (imidazole)), 7.79-7.71 (d, 2H, H4 H5 (imidazole)), 6.37-5.91 (m, 3H, CH_2═CH—), 4.51-4.47 (m, 4H, —O—CH_2—CH_2—N), 3.86 (s, 3H, N—CH_3).

P(MA-S^-)I^+ monomer (1-ethyl-3-methylimidazolium 3-sulfopropyl acrylate) (4): compound 4 was synthesized following the previous research paper.[28] Potassium 3-(acryloyloxy)propane-1-sulfonate (1 eq) and 1-ethyl-3-methylimidazolium chloride (1.2 eq) were dissolved in MeCN. The reaction mixture was stirred overnight at RT. The precipitated salt (KCl) was filtered and the solvent was removed via a rotary evaporator. The crude was redissolved in DCM and kept at < 0 °C overnight. The precipitated salt was filtered and the solvent was removed. A viscous yellow transparent oil product was obtained. ^{1}H NMR (400 MHz, DMSO-d_6): 9.13 (s, 1H, H2 (imidazole)), 7.79-7.70 (d, 2H, H4 H5 (imidazole)), 6.37-5.91 (m, 3H, CH_2═CH—), 4.17 (m, 4H, —O—CH_2—, N—CH_2—), 3.84 (s, 3H, N—CH_3), 2.46 (t, 2H, —CH_2—S), 1.89 (m, 2H, —O—CH_2—CH_2—), 1.41 (t, 3H, N—CH_2—CH_3).

Synthesis of Polymers—Homopolymers: Neutral monomers (MA or S) and AIBN (0.5 mol%) were mixed for polymerization. The solution was degassed by freeze-pump-thaw method and stirred overnight at 70 °C. The crude product was precipitated into methanol.

Synthesis of Polymers—PMA: ^{1}H NMR (400 MHz, DMSO-d_6): 3.57 (s, 3H, —O—CH_3), 1.80-1.59 (m, 3H, —CH_2—CH—).

Synthesis of Polymers—PS: ^{1}H NMR (400 MHz, DMSO-d_6): 7.48-7.27 (m, 5H, —CArH), 2.00-1.43 (m, 3H, —CH_2—CH—).

Synthesis of Polymers—Random Copolymers: Neutral monomers (MA or S), ion monomers (1, 2, 3, 4, or 5), and AIBN (0.5 mol%) were mixed for polymerization. The solution was degassed by freeze-pump-thaw method and stirred overnight at 70 °C.

Synthesis of Polymers—P(MA-A^+_5)$TFSI^-$: MA (0.95 eq) and 1 (0.05 eq) were used for polymerization. ^{1}H NMR (400 MHz, DMSO-d_6): 4.56-4.42 (m, 4H (5%), —O—CH_2—CH_2—N), 3.57 (s, 3H (95%), —O—CH_3), 3.14 (s, 9H (5%), —N—$(CH_3)_3$), 2.32-2.18 (m, 3H (5%), —CH_2—CH—), 1.80-1.57 (m, 3H (95%), —CH_2—CH—).

Synthesis of Polymers—P(MA-A^+_{10})$TFSI^-$: MA (0.9 eq) and 1 (0.1 eq) were used for polymerization. ^{1}H NMR (400 MHz, DMSO-d_6): 4.56-4.42 (m, 4H (10%), —O—CH_2—CH_2—N), 3.57 (s, 3H (90%), —O—CH_3), 3.14 (s, 9H (10%), —N—$(CH_3)_3$), 2.32-2.18 (m, 3H (10%), —CH_2—CH—), 1.80-1.57 (m, 3H (90%), —CH_2—CH—).

Synthesis of Polymers—P(MA-A^+_{20})$TFSI^-$: MA (0.8 eq) and 1 (0.2 eq) were used for polymerization. ^{1}H NMR (400 MHz, DMSO-d_6): 4.56-4.42 (m, 4H (20%), —O—CH_2—CH_2—N), 3.57 (s, 3H (80%), —O—CH_3), 3.14 (s, 9H (20%), —N—$(CH_3)_3$), 2.32-2.18 (m, 3H (20%), —CH_2—CH—), 1.80-1.57 (m, 3H (80%), —CH_2—CH—).

Synthesis of Polymers—P(MA-A^+_{30})$TFSI^-$: MA (0.7 eq) and 1 (0.3 eq) were used for polymerization. ^{1}H NMR (400 MHz, DMSO-d_6): 4.56-4.42 (m, 4H (30%), —O—CH_2—CH_2—N), 3.57 (s, 3H (70%), —O—CH_3), 3.14 (s, 9H (30%), —N—$(CH_3)_3$), 2.32-2.18 (m, 3H (30%), —CH_2—CH—), 1.80-1.57 (m, 3H (70%), —CH_2—CH—).

Synthesis of Polymers—P(MA-S^-_5)K^+: MA (0.95 eq) and 2 (0.05 eq) were used for polymerization in cosolvent (DMF:H_2O = 7:3, v:v). ^{1}H NMR (400 MHz, DMSO-d_6): 4.03 (t, 2H (5%), —O—CH_2—), 3.57 (s, 3H (95%), —O—CH_3), 2.43 (t, 2H (5%), —CH_2—S), 2.32-2.18 (m, 3H (5%), —CH_2—CH—), 1.85 (m, 2H (5%), —O—CH_2—CH_2—), 1.80-1.57 (m, 3H (95%), —CH_2—CH—).

Synthesis of Polymers—P(MA-S^-_{10})K^+: MA (0.9 eq) and 2 (0.1 eq) were used for polymerization in cosolvent (DMF:H_2O = 7:3, v:v). ^{1}H NMR (400 MHz, DMSO-d_6): 4.03 (t, 2H (10%), —O—CH_2—), 3.57 (s, 3H (90%), —O—CH_3), 2.43 (t, 2H (10%), —CH_2—S), 2.32-2.18 (m, 3H (10%), —CH_2—CH—), 1.85 (m, 2H (10%), —O—CH_2—CH_2—), 1.80-1.57 (m, 3H (90%), —CH_2—CH—).

Synthesis of Polymers—P(MA-S^-_{20})K^+: MA (0.8 eq) and 2 (0.2 eq) were used for polymerization in cosolvent (DMF:H_2O = 7:3, v:v). ^{1}H NMR (400 MHz, DMSO-d_6): 4.03 (t, 2H (20%), —O—CH_2—), 3.57 (s, 3H (80%), —O—CH_3), 2.43 (t, 2H (20%), —CH_2—S), 2.32-2.18 (m, 3H (20%), —CH_2—CH—), 1.85 (m, 2H (20%), —O—CH_2—CH_2—), 1.80-1.57 (m, 3H (80%), —CH_2—CH—).

Synthesis of Polymers—P(MA-S^-_{30})K^+: MA (0.7 eq) and 2 (0.3 eq) were used for polymerization in cosolvent (DMF:H_2O = 7:3, v:v). ^{1}H NMR (400 MHz, DMSO-d_6): 4.03 (t, 2H (30%), —O—CH_2—), 3.57 (s, 3H (70%), —O—CH_3), 2.43 (t, 2H (30%), —CH_2—S), 2.32-2.18 (m, 3H (30%), —CH_2—CH—), 1.85 (m, 2H (30%), —O—CH_2—CH_2—), 1.80-1.57 (m, 3H (70%), —CH_2—CH—).

Synthesis of Polymers—P(MA-I^+_5)$TFSI^-$: MA (0.95 eq) and 3 (0.05 eq) were used for polymerization. ^{1}H NMR (400 MHz, DMSO-d_6): 9.09 (s, 1H (5%), H2 (imidazole)), 7.71 (d, 2H (5%), H4 H5 (imidazole)), 4.48-4.35 (m, 4H (5%), —O—CH_2—CH_2—N), 3.86 (s, 3H (5%), N—CH_3), 3.57 (s, 3H (95%), —O—CH_3), 2.32-2.18 (m, 3H (5%), —CH_2—CH—), 1.80-1.57 (m, 3H (95%), —CH_2—CH—).

Synthesis of Polymers—P(MA-I^+_{10})$TFSI^-$: MA (0.9 eq) and 3 (0.1 eq) were used for polymerization. ^{1}H NMR (400 MHz, DMSO-d_6): 9.09 (s, 1H (10%), H2 (imidazole)), 7.71 (d, 2H (10%), H4 H5 (imidazole)), 4.48-4.35 (m, 4H (10%), —O—CH_2—CH_2—N), 3.86 (s, 3H (10%), N—CH_3), 3.57 (s, 3H (90%), —O—CH_3), 2.32-2.18 (m, 3H (10%), —CH_2—CH—), 1.80-1.57 (m, 3H (90%), —CH_2—CH—).

Synthesis of Polymers—P(MA-I^+_{20})$TFSI^-$: MA (0.8 eq) and 3 (0.2 eq) were used for polymerization. ^{1}H NMR (400 MHz, DMSO-d_6): 9.09 (s, 1H (20%), H2 (imidazole)), 7.71 (d, 2H (20%), H4 H5 (imidazole)), 4.48-4.35 (m, 4H (20%), —O—CH_2—CH_2—N), 3.86 (s, 3H (20%), N—CH_3), 3.57 (s, 3H (80%), —O—CH_3), 2.32-2.18 (m, 3H (20%), —CH_2—CH—), 1.80-1.57 (m, 3H (80%), —CH_2—CH—).

Synthesis of Polymers—P(MA-I^+_{30})$TFSI^-$: MA (0.7 eq) and 3 (0.3 eq) were used for polymerization. ^{1}H NMR (400 MHz, DMSO-d_6): 9.09 (s, 1H (30%), H2 (imidazole)), 7.71 (d, 2H (30%), H4 H5 (imidazole)), 4.48-4.35 (m, 4H (30%), —O—CH_2—CH_2—N), 3.86 (s, 3H (30%), N—CH_3), 3.57 (s, 3H (70%), —O—CH_3), 2.32-2.18 (m, 3H (30%), —CH_2—CH—), 1.80-1.57 (m, 3H (70%), —CH_2—CH—).

Synthesis of Polymers—P(MA-S^-_5)I^+: MA (0.95 eq) and 4 (0.05 eq) were used for polymerization in DMF. ^{1}H NMR (400 MHz, DMSO-d_6): 9.13 (s, 1H (5%), H2 (imidazole)), 7.79-7.70 (d, 2H (5%), H4 H5 (imidazole)), 4.20-4.02 (m, 4H (5%), —O—CH_2—, N—CH_2—), 3.85 (s, 3H (5%), N—CH_3), 3.57 (s, 3H (95%), —O—CH_3), 2.46 (t, 2H (5%), —CH_2—S), 2.32-2.18 (m, 3H (5%), —CH_2—CH—), 1.84 (m, 2H (5%), —O—CH_2—CH_2—), 1.80-1.57 (m, 3H (95%), —CH_2—CH—), 1.41 (t, 3H (5%), N—CH_2—CH_3).

Synthesis of Polymers—P(MA-S^-_{10})I^+: MA (0.9 eq) and 4 (0.1 eq) were used for polymerization in DMF. ^{1}H NMR (400 MHz, DMSO-d_6): 9.13 (s, 1H (10%), H2 (imidazole)), 7.79-7.70 (d, 2H (10%), H4 H5 (imidazole)), 4.20-4.02 (m, 4H (10%), —O—CH_2—, N—CH_2—), 3.85 (s, 3H (10%), N—CH_3), 3.57 (s, 3H (90%), —O—CH_3), 2.46 (t, 2H (10%), —CH_2—S), 2.32-2.18 (m, 3H (10%), —CH_2—CH—), 1.84 (m, 2H (10%), —O—CH_2—CH_2—), 1.80-1.57 (m, 3H (90%), —CH_2—CH—), 1.41 (t, 3H (10%), N—CH_2—CH_3).

Synthesis of Polymers—P(MA-S^-_{20})I^+: MA (0.8 eq) and 4 (0.2 eq) were used for polymerization in DMF. ^{1}H NMR (400 MHz, DMSO-d_6): 9.13 (s, 1H (20%), H2 (imidazole)), 7.79-7.70 (d, 2H (20%), H4 H5 (imidazole)), 4.20-4.02 (m, 4H (20%), —O—CH_2—, N—CH_2—), 3.85 (s, 3H (20%), N—CH_3), 3.57 (s, 3H (80%), —O—CH_3), 2.46 (t, 2H (20%),

—CH_2—S), 2.32-2.18 (m, 3H (20%), —CH_2—CH—), 1.84 (m, 2H (20%), —O—CH_2—CH_2—), 1.80-1.57 (m, 3H (80%), —CH_2—CH—), 1.41 (t, 3H (20%), N—CH_2—CH_3).

Synthesis of Polymers—P(MA-S$^-_{30}$)I$^+$: MA (0.7 eq) and 4 (0.3 eq) were used for polymerization in DMF. ^{1}H NMR (400 MHz, DMSO-d_6): 9.13 (s, 1H (30%), H2 (imidazole)), 7.79-7.70 (d, 2H (30%), H4 H5 (imidazole)), 4.20-4.02 (m, 4H (30%), —O—CH_2—, N—CH_2—), 3.85 (s, 3H (30%), N—CH_3), 3.57 (s, 3H (70%), —O—CH_3), 2.46 (t, 2H (30%), —CH_2—S), 2.32-2.18 (m, 3H (30%), —CH_2—CH—), 1.84 (m, 2H (30%), —O—CH_2—CH_2—), 1.80-1.57 (m, 3H (70%), —CH_2—CH—), 1.41 (t, 3H (30%), N—CH_2—CH_3).

Synthesis of Polymers—P(S-S$^-_5$)Na$^+$: S (0.95 eq) and 5 (0.05 eq) were used for polymerization in DI water. Elem. Anal. Calcd: C, 88.67; H, 7.43; S, 1.48; O, 2.21%. Found: C, 86.45; H, 7.32; S, 1.26; O, 2.58%.

Synthesis of Polymers—P(S-S$^-_{10}$)Na$^+$: S (0.9 eq) and 5 (0.1 eq) were used for polymerization in DI water. Elem. Anal. Calcd: C, 85.56; H, 7.13; S, 2.85; O, 4.26%. Found: C, 81.46; H, 7.01; S, 2.52; O, 4.55%.

Synthesis of Polymers—P(S-S$^-_{20}$)Na$^+$: S (0.8 eq) and 5 (0.2 eq) were used for polymerization in DI water. Elem. Anal. Calcd: C, 79.95; H, 6.58; S, 5.32; O, 7.97%. Found: C, 74.16; H, 6.50; S, 4.88; O, 7.66%.

Synthesis of Polymers—P(S-S$^-_{30}$)Na$^+$: S (0.7 eq) and 5 (0.3 eq) were used for polymerization in DI water. Elem. Anal. Calcd: C, 75.02; H, 6.09; S, 7.49; O, 11.21%. Found: C, 65.34; H, 5.73; S, 7.43; O, 11.15%.

Preparation of PE solutions: P(MA-A$^+$)TFSI$^-$ was dissolved in DMF to a concentration of 10 wt%.

P(MA-S$^-$)K$^+$ was dissolved in DI water/DMF (5% and 10%: 3/7, w/w ratio, 20%: 3.5/6.5, w/w ratio, and 30%: 4/6, w/w ratio) and the concentration of the solution was fixed to 10 wt%.

P(MA-I$^+$)TFSI$^-$ was dissolved in DMSO to a concentration of 10 wt%.

P(MA-S$^-$)I$^+$ was dissolved in DMF to a concentration of 10 wt%.

P(S-S$^-$)Na$^+$ was dissolved in DMSO/Toluene (1/1, w/w ratio) and the concentration of the solution was fixed at 10 wt%.

Fabrication of PE-Based TENG: The 500 µL of PE solution was poured onto an indiumtin oxide (ITO)-coated polyethylene terephthalate (PET) (130 µm) substrate, followed by drying in an oven at 80 °C for 12 h to fully remove the residual solvent. The PE layer and triboelectric counter layer (nylon, PET, PI, PFA) were fabricated into a double electrode mode TENG.

Characterizations: ^{1}H NMR (Bruker, AVANCE III 400 MHz) spectra were acquired with DMSO-d_6 as the solvent and tetramethylsilane (TMS) as the internal standard. The compositions of PS-based polyanions were determined by elemental analysis with a Thermo Scientific Flash 2000 Series instrument. The output characteristics of the TENG were measured using a system electrometer (Keithley 6514). The applied force during the TENG measurements was controlled using a Z-axis stage and monitored with a force sensor (DYTRAN 4110c), which was calibrated to ensure accurate force measurement. The dielectric constant and conductivity were measured using an LCR meter (HIOKI, IM3533-01). The surface potential was measured by atomic force microscopy (AFM) (Park Systems, XE7). The chemical characterization of the surface was performed using by time-of-flight secondary ion mass spectrometry (TOF-SIMS) (IONTOF, TOF-SIMS 5–100). The mechanical properties of the polymers were measured using a rheometer (Anton Paar MCR 92).

Supporting Information

Supporting Information is available from the Wiley Online Library or from the author.

Acknowledgements

H.J. and S.P. contributed equally to this work. This research was supported by the Nano & Material Technology Development Program through the National Research Foundation of Korea (NRF) funded by the Ministry of Science and ICT(RS-2024-00451318). This work was supported by the National Research Foundation of Korea (NRF) grant funded by the Korea government. (MSIT) (RS-2024-00448225).

Conflict of Interest

The authors declare no conflict of interest.

Data Availability Statement

The data that support the findings of this study are available from the corresponding author upon reasonable request.

Keywords

polyelectrolyte, stable, triboelectric nanogenerators, tunable tribopolarity platform

Received: March 23, 2025
Revised: May 28, 2025
Published online:

[1] F.-R. Fan, Z.-Q. Tian, Z. L. Wang, *Nano Energy* **2012**, *1*, 328.
[2] a) S. Liu, Y. Li, W. Guo, X. Huang, L. Xu, Y.-C. Lai, C. Zhang, H. Wu, *Nano Energy* **2019**, *65*, 104005; b) Y. Liu, B. Chen, W. Li, L. Zu, W. Tang, Z. L. Wang, *Adv. Funct. Mater.* **2021**, *31*, 2104770.
[3] a) Y. C. Lai, J. Deng, S. L. Zhang, S. Niu, H. Guo, Z. L. Wang, *Adv. Funct. Mater.* **2017**, *27*, 1604462; b) T. Tat, A. Libanori, C. Au, A. Yau, J. Chen, *Biosens. Bioelectron.* **2021**, *171*, 112714.
[4] a) M. Ha, J. Park, Y. Lee, H. Ko, *ACS Nano* **2015**, *9*, 3421; b) F. Wu, C. Li, Y. Yin, R. Cao, H. Li, X. Zhang, S. Zhao, J. Wang, B. Wang, Y. Xing, *Adv. Mater. Technol.* **2019**, *4*, 1800216.
[5] R. Zhang, H. Olin, *EcoMat* **2020**, *2*, 12062.
[6] J. Sun, K. Tu, S. Büchele, S. M. Koch, Y. Ding, S. N. Ramakrishna, S. Stucki, H. Guo, C. Wu, T. Keplinger, *Matter* **2021**, *4*, 3049.
[7] a) J. H. Lee, R. Hinchet, S. K. Kim, S. Kim, S.-W. Kim, *Energy Environ. Sci.* **2015**, *8*, 3605; b) B.-G. Park, C. Lee, Y.-J. Kim, J. Park, H. Kim, Y. Jung, J. S. Ko, S.-W. Kim, J.-H. Lee, H. Cho, *Nano Energy* **2022**, *100*, 107433.
[8] a) X.-S. Zhang, M.-D. Han, R.-X. Wang, B. Meng, F.-Y. Zhu, X.-M. Sun, W. Hu, W. Wang, Z.-H. Li, H.-X. Zhang, *Nano Energy* **2014**, *4*, 123; b) H. Y. Li, L. Su, S. Y. Kuang, C. F. Pan, G. Zhu, Z. L. Wang, *Adv. Funct. Mater.* **2015**, *25*, 5691; c) S.-H. Shin, Y. H. Kwon, Y.-H. Kim, J.-Y. Jung, M. H. Lee, J. Nah, *ACS Nano* **2015**, *9*, 4621.
[9] M. P. Kim, D.-S. Um, Y.-E. Shin, H. Ko, *Nanoscale Res. Lett.* **2021**, *16*, 35.
[10] a) G. Jian, Q. Meng, Y. Jiao, L. Feng, H. Shao, F. Wang, F. Meng, *Chem. Eng. J.* **2021**, *417*, 127974; b) G. Jian, Q. Meng, Y. Jiao, F. Meng, Y. Cao, M. Wu, *Nanoscale* **2020**, *12*, 14160.
[11] a) K. Shi, B. Chai, H. Zou, P. Shen, B. Sun, P. Jiang, Z. Shi, X. Huang, *Nano Energy* **2021**, *80*, 105515; b) J. Wang, H. Wu, Z. Wang, W. He, C. Shan, S. Fu, Y. Du, H. Liu, C. Hu, *Adv. Funct. Mater.* **2022**, *32*, 2204322.
[12] a) V. Harnchana, H. V. Ngoc, W. He, A. Rasheed, H. Park, V. Amornkitbamrung, D. J. Kang, *ACS Appl. Mater. Interfaces* **2018**, *10*, 25263; b) R. Zhang, M. Hummelgård, J. Örtegren, H. Andersson, M. Olsen, D. Chen, J. Li, A. Eivazi, C. Dahlström, M. Norgren, *Nano Energy* **2023**, *115*, 108737.
[13] a) S. Gao, R. Wang, C. Ma, Z. Chen, Y. Wang, M. Wu, Z. Tang, N. Bao, D. Ding, W. Wu, *J. Mater. Chem. A* **2019**, *7*, 7109; b) Z. Sha, C. Boyer, G. Li, Y. Yu, F.-M. Allioux, K. Kalantar-Zadeh, C.-H. Wang, J. Zhang, *Nano Energy* **2022**, *92*, 106713.
[14] a) H. Joo, S. Gwak, H. Park, H.-J. Yoon, H. Ryu, S. A. Han, J.-H. Lee, *Nano Energy* **2024**, *126*, 109706; b) H. J. Hwang, K. Y. Kim, J. S. Kim, T. Kim, D. H. Kim, Y. Lee, D. Choi, *Nano Energy* **2024**, *125*, 109535.
[15] a) L. Sun, S. Chen, Y. Guo, J. Song, L. Zhang, L. Xiao, Q. Guan, Z. You, *Nano Energy* **2019**, *63*, 103847; b) Y. Lee, S. Lim, W. J. Song, S. Lee, S.

J. Yoon, J. M. Park, M. G. Lee, Y. L. Park, J. Y. Sun, *Adv. Mater.* **2022**, *34*, 2108586.
[16] a) P. Lv, L. Shi, C. Fan, Y. Gao, A. Yang, X. Wang, S. Ding, M. Rong, *ACS Appl. Mater. Interfaces* **2020**, *12*, 15012; b) Y. Wu, Y. Luo, T. J. Cuthbert, A. V. Shokurov, P. K. Chu, S. P. Feng, C. Menon, *Adv. Sci.* **2022**, *9*, 2106008; c) P. Nellepalli, M. P. Kim, J. Park, S. M. Noh, Z. Ye, H. W. Jung, H. Ko, J. K. Oh, *ACS Appl. Mater. Interfaces* **2022**, *14*, 17806.
[17] H. J. Hwang, J. S. Kim, W. Kim, H. Park, D. Bhatia, E. Jee, Y. S. Chung, D. H. Kim, D. Choi, *Adv. Energy Mater.* **2019**, *9*, 1803786.
[18] D. L. Vu, C. P. Vo, C. D. Le, K. K. Ahn, *Int. J. Energy Res.* **2021**, *45*, 8960.
[19] Y. Kim, D. Lee, J. Seong, B. Bak, U. H. Choi, J. Kim, *Nano Energy* **2021**, *84*, 105925.
[20] X. Zhao, Z. Ounaies, *Nano Energy* **2022**, *94*, 106908.
[21] S. K. Ghosh, M. P. Kim, S. Na, Y. Lee, J. Park, S. Cho, J. Cho, J. J. Kim, H. Ko, *Nano Energy* **2022**, *100*, 107438.
[22] F. Ou, T. Xie, X. Li, Z. Zhang, C. Ning, L. Tuo, W. Pan, C. Wang, X. Duan, Q. Liang, *Mater. Horiz.* **2024**, *11*, 2191.
[23] a) Y. Wu, Y. Luo, J. Qu, W. A. Daoud, T. Qi, *Nano Energy* **2020**, *75*, 105027; b) X. He, H. Cheng, S. Yue, J. Ouyang, *J. Mater. Chem. A* **2020**, *8*, 10813.
[24] M. Li, H.-W. Lu, S.-W. Wang, R.-P. Li, J.-Y. Chen, W.-S. Chuang, F.-S. Yang, Y.-F. Lin, C.-Y. Chen, Y.-C. Lai, *Nat. Commun.* **2022**, *13*, 938.
[25] a) X. Kang, C. Pan, Y. Chen, X. Pu, *RSC Adv.* **2020**, *10*, 17752; b) H. Joo, S. Gwak, M. H. Lee, H. Park, C. Lee, J. H. Lee, S. A. Han, J.-H. Lee, *Sustainable Mater. Technol.* **2023**, *36*, 00638.
[26] S. Weigold, M. Spyridakou, I. Tzourtzouklis, J. Freudenberg, U. H. Bunz, K. Müllen, G. Floudas, *ACS Appl. Nano Mater.* **2024**, *7*, 16256.
[27] a) P. Wang, S. M. Zakeeruddin, P. Comte, I. Exnar, M. Grätzel, *J. Am. Chem. Soc.* **2003**, *125*, 1166; b) W. Kubo, T. Kitamura, K. Hanabusa, Y. Wada, S. Yanagida, *Chem. Commun.* **2002**, 374; c) N. Sun, X. Gao, A. Wu, F. Lu, L. Zheng, *J. Mol. Liq.* **2017**, *248*, 759.
[28] H. J. Kim, B. Chen, Z. Suo, R. C. Hayward, *Science* **2020**, *367*, 773.